Ultrasonics Sonochemistry 90 (2022) 106181

Contents lists available at ScienceDirect

Ultrasonics Sonochemistry

journal homepage: www.elsevier.com/locate/ultson

Medium-high frequency sonication dominates spherical-SiO_2 nanoparticle size

Xiaolin Liu, Zhilin Wu *, Maela Manzoli, László Jicsinszky, Roberta Cavalli, Luigi Battaglia, Giancarlo Cravotto *

Department of Drug Science and Technology and NIS—Centre for Nanostructured Interfaces and Surfaces, University of Turin, Via Pietro Giuria 9, 10125 Turin, Italy

ARTICLE INFO

Keywords:
Stöber method
Spherical SiO_2 nanoparticles
Sonication
Medium-high frequencies
Number and size of cavitation bubbles

ABSTRACT

Spherical SiO_2 nanoparticles (SSNs) have been inventively synthesized using the Stöber method with sonication at medium–high frequencies (80, 120, and 500 kHz), aiming to control SSN size and shorten reaction time. Compared to the conventional method, such sonication allowed the Stöber reaction complete in 20–60 min with a low molar ratio of NH_4OH/tetraethyl orthosilicate (0.84). The hydrodynamic diameters of 63–117 nm of SSNs were obtained under sonication with 80, 120, and 500 kHz of ultrasonic frequencies. Moreover, the SSNs obtained were smaller at 120 kHz than at 80 kHz in a multi-frequencies ultrasonic reactor, and the SSN size decreased with increasing ultrasonic power at 20 °C, designating the sonochemical unique character, namely, the SSN-size control is associated with the number of microbubbles originated by sonication. With another 500 kHz ultrasonic bath, the optimal system temperature for producing smaller SSNs was proven to be 20 °C. Also, the SSN size decreased with increasing ultrasonic power. The smallest SSNs (63 nm, hydrodynamic diameter by QELS, or 21 nm by FESEM) were obtained by sonication at 207 W for 20 min at 20 °C. Furthermore, the SSN size increased slightly with increasing sonication time and volume, favoring the scale-up of SSNs preparation. The mechanisms of controlling the SSN size were further discussed by the radical's role and effects of ammonia and ethanol concentration.

1. Introduction

Spherical SiO_2 nanoparticles (SSNs) are widely applied in biomedical fields including biosensors, DNA transfection, cancer treatment, etc [1–3]. The Stöber process, via the hydrolysis and polycondensation of tetraethyl orthosilicate (TEOS) in alkaline ethanol (Scheme. 1), is a common method for the preparation of monodisperse SSNs [4,5]. In the conventional process, SSN size is modulated by many factors, such as the ethanol/NH_4OH/TEOS/H_2O ratio, reaction temperature and time, etc.

Ismai *et al.* explored the effects of TEOS (0.2–0.4 mol/L) and ammonia (0.11–0.3 mol/L) concentrations on SSN size [6]. Both the hydrolysis and condensation rates become faster with increasing TEOS and ammonia concentrations, producing fewer nuclei and larger particle size. Under the optimal conditions, 50 nm silica particles were obtained with 0.2 mol/L ammonia and 0.2 mol/L TEOS at ambient temperature for 24 hrs. Wang *et al.* also studied the effect of TEOS (0.22–1.115 mol/L) and ammonia concentrations on silica particle size in the mixture of water and isopropanol [7]. With a constant NH_4OH/TEOS molar ratio (0.81), 30 nm or 860 nm silica particles were obtained with 0.22 mol/L or 1.115 TEOS at 20 °C for 5 hrs, respectively. As a catalyst, higher ammonia accelerates the hydrolysis and condensation and promotes the production of more oligomers to form larger particles. It is conspicuous that smaller SSNs are obtained with the lower NH_4OH/TEOS molar ratio, but long reaction times (5–24 hrs) are required, whereas the higher reaction rate with the higher NH_4OH/TEOS molar ratio leads to larger particle sizes (ca. 800 nm) [5]. The sonochemical method has long been used in the preparation of nanoparticles and nanocrystals to accelerate the synthesis and reduce nanoparticle size [8–11]. Ultrasonic cavitation is generally regarded as the origin of sonochemistry, namely, the implosion of cavitation microbubbles generates extremely high local temperature and pressure, high-speed microjets, strong shock waves, and shear forces, which contribute to the fabrication of nanostructured materials [12,13]. The number and size of cavitation bubbles are also critical for the fabrication of nanostructured materials. The cavitation bubble surfaces can act as crystal nucleation sites, leading to increasing nucleation rates [14–16]. Therefore, the reduction in crystal size and the

* Corresponding authors.
E-mail addresses: zhilin.wu@unito.it (Z. Wu), giancarlo.cravotto@unito.it (G. Cravotto).

https://doi.org/10.1016/j.ultsonch.2022.106181
Received 29 July 2022; Received in revised form 22 September 2022; Accepted 24 September 2022
Available online 27 September 2022

narrowness of the crystal size distribution can be explained by the number of cavitation bubbles induced by sonication. Specifically, the number of cavitation bubbles increases with increasing ultrasonic frequency and power, resulting in increasing number of crystal nuclei [17,18]. Moreover, the activity of cavitation bubbles is substantially dependent on the bubbles size, which decreases with increasing ultrasonic frequency, but the bubbles size increases with increasing ultrasonic power [19–23]. In 1996, Enomoto *et al.* attempted to improve the Stöber process using sonication at 20 kHz and 1.9–25.4 W cm^{-2} for 90 min at 20 °C [24]. With 3.0 mol/L ammonia and 0.1 mol/L TEOS (NH_4OH/TEOS molar ratio: 30), however, larger SSN sizes (330–380 nm) were obtained by sonication compared to the 310 nm SSNs produced without sonication. This behavior was explained by the presence of sonication-induced agglomeration. In 2018, Lin *et al.* reported the rapid synthesis of silica particles by ultrasound-assisted Stöber method [25]. With 1.36 mol/L ammonia and 0.58 mol/L TEOS (NH_4OH/TEOS molar ratio: 2.34) in 46 mL of reaction mixture, ca. 615 nm silica particles were obtained by 25 kHz sonication at 160 W for 5 min and stirred at 999 rpm simultaneously. In 2022, Kamila *et al.* found that the larger silica particles are generated by sonochemical method as compared with the sol–gel Stöber method again [26]. In the preparation, the Stöber mixture containing 2.85 mol/L ammonia and 1 mol/L TEOS (NH_4OH/TEOS molar ratio: 2.85) with ethanol and water was stirred at 450 rpm for 90 min at room temperature, or sonicated with an ultrasonic probe for 30 min (5 s pulse on and 2 s pulse off). The average particle sizes obtained by the conventional sol–gel or sonochemical Stöber method were 223 nm or 398 nm, respectively.

In contrast, Rahman *et al.* obtained 93 nm SSNs by the Stöber method with sonication at 42 kHz for 7 hrs at ca. 45 °C, however, it was just comparable to those generated using magnetic agitation with 1.87 mol/L ammonia and 0.7 mol/L TEOS (NH_4OH/TEOS molar ratio:2.67) [27]. In 2009, Yao *et al.* reported the preparation of 80 nm SSNs with 4.89 of NH_4OH/TEOS molar ratio using sonochemical method [28]. The mixture containing 8 mL of ammonia and 2.5 mL of TEOS with ethanol, water, and dye thionine was sonicated at 20 kHz and 100 W cm^{-2} for 30 min under ambient air. To obtain smaller SSNs, furthermore, the NH_4OH/TEOS molar ratio was decreased to 0.25 in a Stöber mixture containing 1 mL of ammonia and 6.3 mL of TEOS with ethanol, water, and a certain amount of PEG 1000 [29]. The reaction was carried out with ultrasonic vibration for 5.5 hrs at 45 °C. In addition, some post-treatments, such as aging and calcination, were performed to achieve an average size of 9 nm.

To date, the ultrasonic frequencies applied for the sonochemical preparation of silica particles were between 20 and 42 kHz, leading to larger silica particles (mostly over 300 nm and rarely below 50 nm). Also, most ultrasonic treatment time is more than 1 hr. Therefore, the proposed advantages of sonication, i.e., reducing SSN size and reaction time, are not evident at low frequencies. In this work, the Stöber reaction mixture has been sonicated at medium–high frequencies (80, 120, and 500 kHz) to obtain smaller SSN sizes in up to 1 hr reaction. The effects of ultrasonic frequency and power, temperature, sonication time, and reaction volume on SSN size and yield under a static air atmosphere have been investigated. The roles of the size and number of cavitation microbubbles, the radicals initiated under sonication, and the concentration of ammonia and ethanol in modulating SSN size are discussed.

2. Methods

2.1. Materials

TEOS (98.0 %, Aldrich), ethanol (≥99.8 %, Sigma-Aldrich), NH_4OH (30.0 %, Carlo Erba), *n*-Butanol (98.0 %, E. Merck, Darmstadt) were used without additional purification.

2.2. Experimental devices

A low-frequency ultrasonic device (20 kHz) consists of an ultrasonic generator (Maximum electrical output power: 70 W) equipped with a titanium horn (tip diameter: 13 mm) and a 20-mL cylindrical glass reactor (HNG-20500-SP, Hainertec (Suzhou) Co., ltd, China). The reaction temperature was controlled by an ice bath. The diagram of the setup refers to our previous work [30]. A multi-frequency device (40, 80 and 120 kHz) consists of a sonic digital cleaning generator (Maximum electrical output power: 150 W) and a 5.6-L ultrasonic bath (28 cm × 20 cm × 10 cm) equipped with cooling water serpentine at 1 cm from the bottom (MG 200, Weber Ultrasonics, Germany, Fig. 1A). A high-frequency device (500 kHz) consists of an ultrasonic cleaning generator (Maximum electrical output power: 250 W) and a 5.6-L ultrasonic bath (28 cm × 20 cm × 10 cm) equipped with cooling water serpentine at 1 cm from the bottom (UMC, Weber Ultrasonics, Germany, Fig. 1B). The ultrasonic powers delivered were determined calorimetrically with water as heating media and all ultrasonic power mentioned below refers to the power measured calorimetrically [31]. As a conventional method, a 20-mL cylindrical glass reactor placed on a magnetic stirrer (AREX VELP Scientifica, Italy) was also used to prepare SSNs at room temperature for comparison. A centrifuge (Allegra 64R Benchtop Centrifuge, Beckman Coulter, Italy) was used to collect the prepared SSNs from reaction systems and washing liquids. The SSNs were collected with the centrifuge (20,000 rpm, 15 min) and washed twice with ethanol and then washed once with distilled water.

2.3. Typical runs of SSNs preparation.

All the preparation of SSNs was carried out under an air atmosphere. The sonochemical processes of the SSNs preparation with various ultrasonic reactors are described as follows:

(A) SSNs preparation using sonication at 20 kHz: 6.00 mL of 99.8 % ethanol, 3.00 mL H_2O and 0.25 mL of TEOS were added to a 20-mL cylindrical reactor (ID: 25 mm) in turn. Subsequently, 0.40 mL of 8.1 % NH_4OH as a catalyst was added to the above mixture, so that the molar ratio of 99.8 % ethanol/8.1 % NH_4OH/TEOS/H_2O was 92.92/0.84/1.00/150.89. Then, ca. 10 mL of the above reaction mixture was

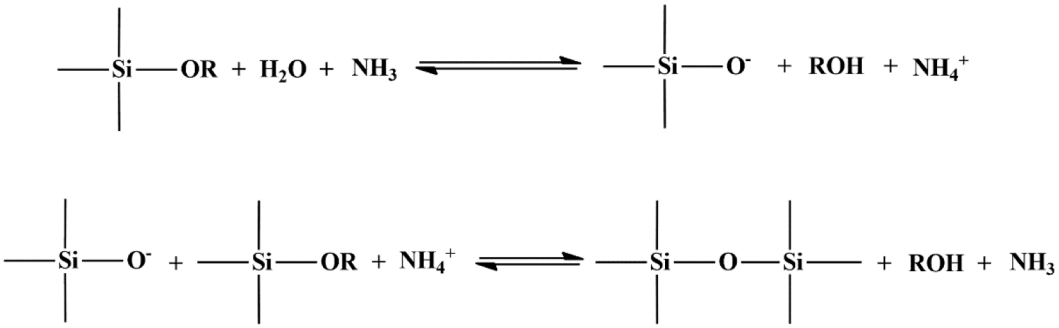

Scheme 1. Stöber preparation of monodisperse SSNs by hydrolysis and condensation of TEOS [3].

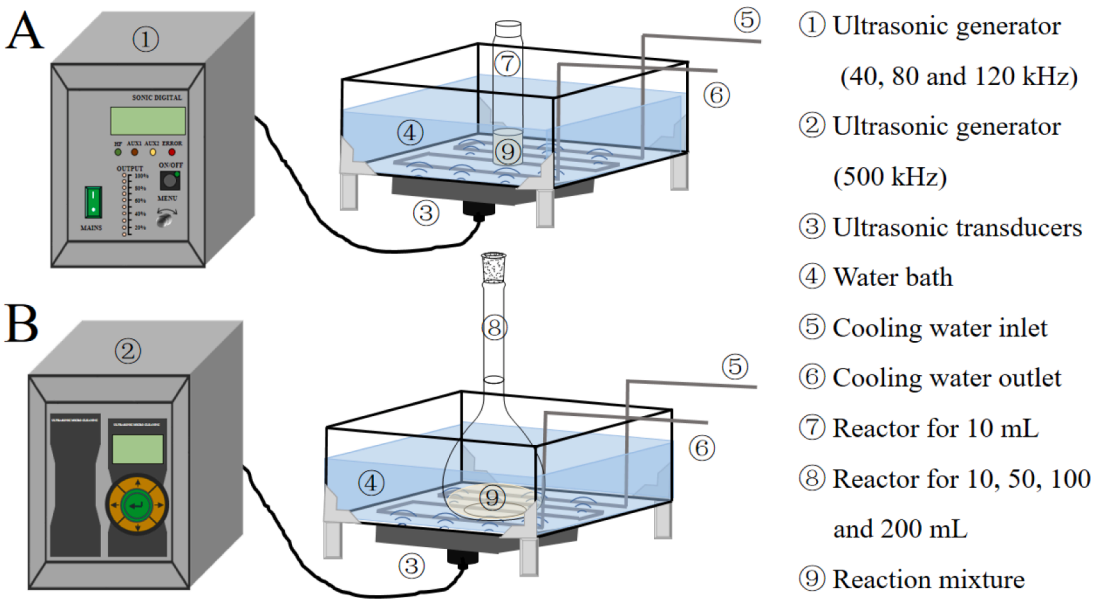

Fig. 1. Setups for sonication with ultrasonic generators and baths (A) 40, 80, and 120 kHz; (B) 500 kHz.

sonicated using an ultrasonic horn with 20 kHz and 40 W for 60 min at 20℃ in an ice bath. The ultrasonic power density and power intensity were calculated to be 4.15 W mL^{-1} and 30.15 W cm^{-2}, respectively. For comparison, ca. 10 mL of the same reaction mixture as above was stirred using a magnetic stirrer with 450 rpm at 20℃ for 24 hrs.

(B) SSNs preparation using sonication at 40, 80 and 120 kHz: 3 L of water as an ultrasonic medium was placed in a 5.6-L ultrasonic bath. Firstly, the degassing was performed for 20 min with sonication and the temperature of ultrasonic bath was maintained at 20 ± 0.3 °C with cooling water. 10 mL of the same reaction mixture as above in 40-mL cylindrical reactor (ID: 25 mm) was sonicated with different ultrasonic frequencies and powers (40 kHz: 97 W; 80 kHz: 17–63 W; 120 kHz: 17–78 W) at 20℃ for 20 min respectively.

(C) SSNs preparation using sonication at 500 kHz: The same ultrasonic medium and the temperature control as above were applied in a 500 kHz ultrasonic bath. The same reaction mixtures as above with different volumes (10–200 mL) were sonicated with different ultrasonic powers (63–207 W) at 15-35℃ for 20–60 min, respectively.

2.4. Characterization of SSNs

The collected SSNs were dispersed in 4 mL of distilled water. 1 mL of the above SSNs dispersion was centrifuged and oven-dried at 45℃ to measure yield with the weighing method. The remaining 3 mL of the SSNs dispersion was used for particle size analysis with Quasi Elastic Light Scattering (QELS). Unless otherwise specified, the SSN size mentioned herein refers to the hydrodynamic SSN size determined by QELS. After the measurement with QELS, the white SSNs were collected by centrifugation (20,000 rpm for 15 min) and lyophilized for the further characterization with Field Emission Scanning Electron Microscope (FESEM), Fourier-transform infrared spectroscopy (FT-IR), Powder X-ray diffraction (PXRD), and Thermogravimetric analysis (TGA), etc.

The particle sizes of SSNs were measured via a QELS method at 25 °C using particle sizing Brookhaven Instruments (Holtsville, NY, USA) with the software of 90plus/BI-MASS. The scattering angle and operating wavelength were 90° and 675.0 nm, respectively. The samples were measured in water. Ultra-high resolution FESEM measurements were performed on a Tescan S9000G FESEM 3010 microscope (30 KeV) equipped with a high-brightness Schottky emitter. For analysis, the powder samples were deposited on a stub coated with a conducting adhesive and inserted in the chamber by a fully motorized procedure. The FT-IR spectra (Spectrum Two, PerkinElmer, USA) were measured by a spectrometer from 500 to 4000 cm^{-1} at 2 cm^{-1} resolution with 64 scans. PXRD patterns were collected with a PW3050/60 X'Pert PRO MPD diffractometer from PANalytical working in Bragg–Brentano geometry, using as a source the high-powered ceramic tube PW3373/10 LFF with a Cu anode (Cu Kα1 radiation $\lambda = 1.5406$ Å) equipped with a Ni filter to attenuate K_β. Scattered photons were collected by a real-time multiple strip (RTMS) X'celerator detector. Data were collected in the $5° \leq 2\theta \leq 90°$ angular range, with 0.02° 2θ steps. The powdered sample was examined in its as-received form and posed in a spinning sample holder to minimize the preferred orientations of crystallites. TGA was used to measure the thermal stability of SSNs. About 10 mg of sample was heated to 1000 °C under a nitrogen atmosphere with airflow of 20 mL min^{-1}. In the first step, the temperature increased from 35 °C to 120 °C with a heating rate of 10 °C min^{-1} and held at 120 °C for 10 min. In the second step, the temperature increased from 120 °C to 800 °C with 20 °C min^{-1}, and held at 800 °C for 10 min. In the third step, the temperature increased from 800 °C to 1000 °C with 20 °C min^{-1}, and maintained at 1000 °C for 5 min.

3. Results and discussion

The physical effects of ultrasonic cavitation, such as local temperature and pressure, shear stress, shock wave, microjet, etc., favor the mass transfer and heat transfer, in particular, promote the reactions in the heterogeneous systems. TEOS is poorly soluble in water, but is miscible with alcohol [32]. Ammonia is very volatile, meaning that both TEOS and ammonia may accumulate on the surface of the cavitation bubbles, accelerating the hydrolysis and condensation of TEOS around the active cavities [33]. Probably, the radicals generated under sonication are also involved in the above reactions [34]. Thus, the sonication can be employed to enhance the hydrolysis and condensation of TEOS [35]. It was possible to produce the smaller SSNs when the reactant ratios were optimized, in particular, when reducing the ammonia concentration during sonication [27,34]. In our preliminary study for optimizing the reactant ratio, the Box-Behnken response surface methodology was applied. The experiment was designed and optimized with Design Expert 12.0 statistical software (free trial version 12.0, Stat-Ease, Inc., USA). Approximate 10 mL of the Stöber reaction mixture with various reactants ratios was sonicated at 120 kHz and 78 W for 20 min at 20 °C.

As a result, the smallest SSNs (average size: 71 nm) were obtained with the optimized Stöber mixture (99.8 % ethanol: 6.00 mL, 8.1 % NH_4OH: 0.40 mL, 98.0 % TEOS: 0.25 mL, H_2O: 3.00 mL). The optimal reactant volume ratio was: ethanol/NH_4OH/TEOS/H_2O = 24.0/1.6/1.0/12.0, which is equivalent to a molar ratio of 92.92/0.84/1.00/150.89 (Table S1 and Fig. S1).

3.1. Effects of ultrasonic frequency and power on SSN size and yield

With the optimal reactant ratio obtained in the above study, ca. 10 mL of the above reaction mixture was either stirred or sonicated at lower frequencies (20 and 40 kHz) at 20 °C. During 24 hrs of agitation (450 rpm), unfortunately, the reaction mixture always appeared clear and transparent state, and no white suspension appeared. The same phenomenon was observed during 20 kHz sonication with an ultrasonic horn at 40 W for 60 min. It is speculated that the NH_4OH/TEOS molar ratio (0.84) used in the above Stöber mixtures was lower as compared with those (NH_4OH/TEOS molar ratio: 2.33–30.00) reported in previous studies [24–27]. In contrast, SSNs were produced under the 40 kHz sonication at 97 W for 20 min in a ultrasonic bath, but the preparation reproducibility was poor. The follow-up studies, therefore, focused on medium–high frequency (80 and 120 kHz, and 500 kHz) with two ultrasonic baths, respectively. Due to the difference in their structures and power ranges of ultrasonic reactors, unfortunately, the results obtained using the 500 kHz ultrasonic bath could not be compared with results obtained using the multi-frequencies (40–120 kHz) ultrasonic bath.

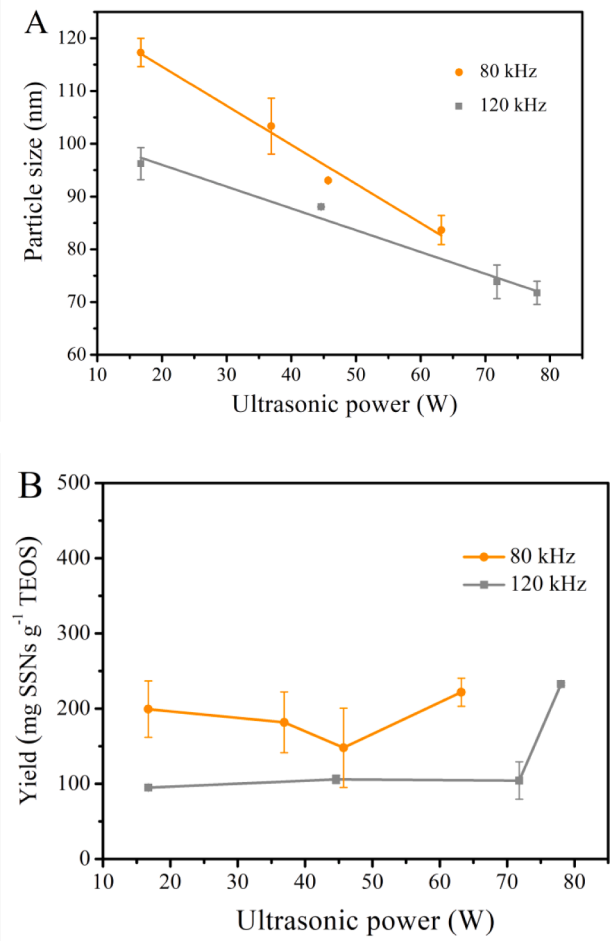

Fig. 2. Dependence of SSN hydrodynamic diameter size by QELS (A) and yield (B) on ultrasonic power at 80 and 120 kHz. Conditions: ca. 10 mL of mixture (99.8 % ethanol: 6.00 mL; 8.1 % NH_4OH: 0.40 mL; 98.0 % TEOS: 0.25 mL; H_2O: 3.00 mL) was sonicated for 20 min at 20 °C in a 3 L water bath.

Fig. 2A and B show the effects of the ultrasonic frequency and power on the SSN size and yield obtained in the multi-frequency ultrasonic bath (80 and 120 kHz), respectively. As shown in Fig. 2A, the SSN sizes obtained at 120 kHz were distinctly smaller than those obtained at 80 kHz and the SSN size decreased with increasing ultrasonic powers. Under sonication, the relationship between SSN sizes and ultrasonic power with various frequencies can be well fitted by the linear equation, as follows:

$$d_{80kHz} = -0.741 \times P_{US} + 129.44, \quad R^2 = 0.978 \tag{1}$$

$$d_{120Hz} = -0.413 \times P_{US} + 104.28, \quad R^2 = 0.975 \tag{2}$$

where d_{80kHz} and d_{120kHz} are the hydrodynamic diameters of SSNs obtained at 80 and 120 kHz; P_{US} is the ultrasonic power.

In terms of Eqs. (1) and (2), the slope (0.741) obtained by 80 kHz is higher than that (0.413) obtained by 120 kHz, indicating that the effect of ultrasonic power on SSN size is more profound at 80 kHz than at 120 kHz. At 80 kHz, the hydrodynamic SSN sizes decreased from 117 to 84 nm with increasing ultrasonic power (17–63 W). At 120 kHz, the SSN sizes decreased from 92 to 72 nm with increasing ultrasonic power (17–78 W).

In Fig. 2B, the SSN yields at 120 kHz were obviously lower than those obtained at 80 kHz. At lower power settings, SSN yields slightly decreased at 80 kHz as ultrasonic power increased, while the yields changed minimally at 120 kHz. At the highest ultrasonic power, SSN yields increased sharply at 80 and 120 kHz. This unpredictable result may be caused by the complex effects of ultrasonic frequency and power, which should be further explored in the future. Fig. 3 shows the dependence of the SSN size and yield obtained on the ultrasonic power in a high-frequency ultrasonic bath (500 kHz).

As shown in Fig. 3, the SSN sizes obviously decreased with increasing ultrasonic power. Under 500 kHz sonication, the relationship between SSN sizes and ultrasonic power can be also well fitted by the linear Eq. (3). In terms of Eq. (3), the slope (0.185) obtained by 500 kHz is quite low, indicating that the effect of ultrasonic power on SSN size is relatively less at 500 kHz. The smallest SSNs (63 nm by QELS, or 21 nm by FESEM) were obtained by sonication at 500 kHz and 207 W for 20 min at 20 °C. Moreover, the yield of SSNs linearly decreased with increasing power and reached a minimum value at 207 W (155 mg SSNs g^{-1} TEOS), as shown in Eq. (4):

$$d_{500kHz} = -0.185 \times P_{US} + 100.31, \quad R^2 = 0.991 \tag{3}$$

$$Y_{500kHz} = -0.764 \times P_{US} + 320.51, \quad R^2 = 0.952 \tag{4}$$

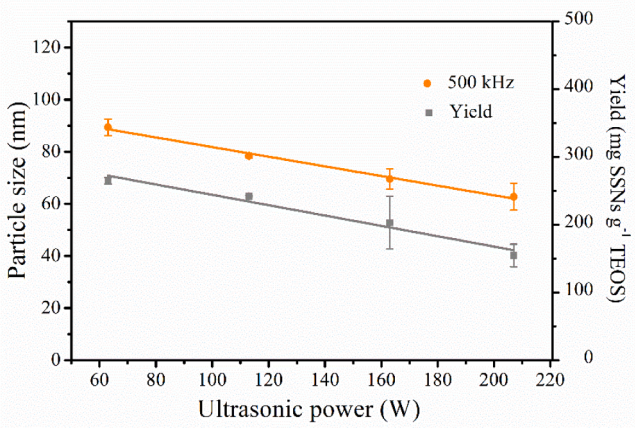

Fig. 3. Dependence of SSN hydrodynamic diameter size by QELS and yield on ultrasonic power at 500 kHz. Conditions: ca. 10 mL of mixture (99.8 % ethanol: 6.00 mL; 8.1 % NH_4OH: 0.40 mL; 98.0 % TEOS: 0.25 mL; H_2O: 3.00 mL) was sonicated for 20 min at 20 °C in a 3 L water bath.

where d_{500kHz} is the hydrodynamic diameters of SSNs obtained at 500 kHz; P_{US} is the ultrasonic power; $Y_{500\ kHz}$ is the yield of SSNs obtained at 500 kHz.

In general, the smaller bubbles cause Rayleigh contraction, whereas larger bubbles are not involved in the sonochemical reaction [27]. Sonication with medium–high frequencies (80–1100 kHz) generated more numerous and smaller microbubbles than that at low frequencies (20–42 kHz), thus increasing the number of active bubbles, which refer to active bubbles with the optimal sizes that can produce stronger physical and chemical phenomena, such as reactive oxygen species, sonoluminescence, sonochemluminescence, etc. [18–20,36,37]. In addition, the amount of water vapor trapped inside bubbles at the collapse decreases with increasing ultrasonic frequency, resulting in highly active bubbles, meaning that those inactive bubbles became active and those active bubbles turned into more active [38]. Consequently, the number of "active bubbles" remarkably increased under the sonication with the higher frequencies, leading to smaller SSNs.

In 1999, Burdin *et al.* reported that active bubbles have a typical radius of 8 μm by 20 kHz sonication as determined by laser light diffraction [39]. Also, it was reported that the average bubble radius (135 μm) at 20 kHz was about 6.8 times of that (20 μm) at 40 kHz, while the average number of bubbles at 40 kHz was about 4.6 times of that at 20 kHz [40]. In 2002, Yasui calculated the range of the ambient bubble radius with increasing ultrasonic frequency, i.e., 0.1–100 μm, 0.1–10 μm, and 0.1–3 μm at 20, 140 and 1000 kHz [38]. In 2005, Lee *et al.* and Brotchie *et al.* summarized that the ranges of bubble size created by 20, 515, and 1100 kHz in water were 2.0–25.0, 2.8–3.7, and 0.9–1.38 μm, respectively [19,21]. In 2021, Yasui reported the ambient bubble radii generated under various frequencies, i.e., 5 μm for 20 kHz, 3.5 μm for 100 and 300 kHz, and 1 μm for 1 MHz [23]. In particular, both the bubble dynamics and the bubble size are very similar between high frequencies [41]. In 2009, Brotchie *et al.* reported that the ambient bubble radii in the frequency range of 200–650 kHz, i.e., 3.9, 3.2, and 2.9 μm for 213, 355, and 647 kHz, respectively [19]. In 2013, Merouani *et al.* summarized the mean measured bubble radius induced by various medium–high frequencies, i.e., 3.9–8.0 μm at 213–230 kHz, 3.2–7.0 μm at 355–350 kHz, 2.8–4.3 μm at 515 kHz, 2.7 μm at 860 kHz, and 0.9–2.0 μm at 1000–1140 kHz [20,42]. In 2021, Dehane *et al.* reported that the optimum ambient bubble radius (3.1 and 2.4 μm) was achieved at 300 and 515 kHz [43]. Moreover, the number of bubbles depends strongly on the operating parameters of the sonication [44,45]. The increasing ultrasonic frequency leads to a substantial increase in the number of bubbles formed in the reactor [42]. Pétrier *et al.* reported the number of active bubbles, i.e., 0.73–1.1 × 10^4, 5.2–5.4 × 10^6, 3.7–5.3 × 10^7, and 6.4–9.1 × 10^7N (L^{-1} s^{-1}) created by 20, 200, 500, and 800 kHz [44,45]. Merouani *et al.* reported the number of active bubbles, i.e., 2.8 × 10^7, 3.9 × 10^8, 3.0 × 10^9, and 3.1 × 10^9N (L^{-1} s^{-1}) created by 300, 585, 860, and 1140 kHz [42]. Therefore, the number of bubbles increases with the frequency increase while the size of bubbles decreases. It is inferred that the size of SSNs may be controlled by the number of bubbles and the size of the bubbles, as shown in Fig. 2A.

On the other hand, increasing ultrasonic power resulted in more numerous and larger microbubbles [19,20,23,36,46]. It has been demonstrated that the optimal ambient radius increased linearly with increasing acoustic amplitude up to 3 atm. However, slight minima of optimal radius were observed for the curves obtained at 500 and 1000 kHz [20]. In 2016, Merouani and Hamdaoui studied the effect of power intensity on the optimum ambient bubble radius created with various medium–high frequencies, i.e, at 140, 515, and 1000 kHz, 11.1, 2.5, and 1.5 μm with 0.75 W cm^{-2}, while 13.25, 3.0, and 1.6 μm with 1 W cm^{-2}, respectively [36]. As shown in Figs. 2A and 3, the SSN size generally decreased with increasing ultrasound power. Combining the effect of the ultrasonic frequency on the particle size of SSNs, it can be speculated that the SSN size is mainly controlled by the number of active bubbles, not by the size of bubbles, as TEOS and ammonia are more evenly distributed around the larger number of active bubbles. Therefore, smaller SSNs were generated with increasing ultrasonic powers, and the smallest SSNs (63 nm) were achieved by 500 kHz sonication at highest ultrasonic power (207 W).

As shown in Fig. 2B, the yields of SSNs obtained at 120 kHz were significantly lower than those obtained at 80 kHz within a comparable ultrasonic power range. For the given amounts of TEOS and ammonia in the reaction system, the number of cavitation bubbles increased with increasing ultrasonic frequencies, resulting in better dispersion of TEOS and ammonia and the decreasing concentration at nucleation sites, thereby the lower yield. At 500 kHz, the yield of SSNs decreased with increasing power and reached a minimum value at 207 W (155 mg SSNs g^{-1} TEOS). Similar to the effect of frequency, the larger number of active bubbles were generated as the increasing power, leading to TEOS and ammonia being more dispersed, thereby decreasing the yield of SSNs.

3.2. Influence of reaction volume on SSN size and yield

As presented above, the smallest SSNs (63 nm) and the corresponding yields (155 mg SSNs g^{-1} TEOS) were obtained in ca. 10 mL of reaction mixture sonicated at 500 kHz, 207 W for 20 min at 20 °C. In the larger reaction volume (ca. 50 mL), however, the reaction mixture always appeared clear and transparent state, and no white suspension appeared during 20 min of sonication. To scale up SSN synthesis, the sonication time was extended to 60 min for each batch of reaction. The influence of sonication time on SSN size and yield will be discussed in Section 3.4. 50–200 mL of the reaction mixture was sonicated at 500 kHz, 207 W for 60 min at 20 °C, respectively. Fig. 4 shows that the sizes and yields of the SSNs prepared at larger volumes.

The average hydrodynamic sizes of SSNs reached 66, 68, and 77 nm in 50, 100, and 200 mL, respectively, which are 5–23 % higher than those (63 nm) prepared in 10 mL of the reaction mixture. It suggests that SSN-synthesis scale-up is feasible in the same ultrasonic reactor, and the synthesis efficiency very slightly fluctuates over the 50–200 mL range.

3.3. Dependence of SSN size and yield on the system temperature

The cavity number, size, collapse intensity and local temperature, and sonochemical efficiency are strongly dependent on bulk-liquid temperature [46,47]. Fig. 5 shows that a larger SSN size and higher yield were achieved at 15 °C than at 20 °C under 60 min sonication at 500 kHz and 207 W. Upon increasing the temperature further, a few SSNs were produced at 25 °C. More surprisingly, the reaction mixture always appeared clear and transparent state and no white suspension appeared during 60 min sonication at 35 °C.

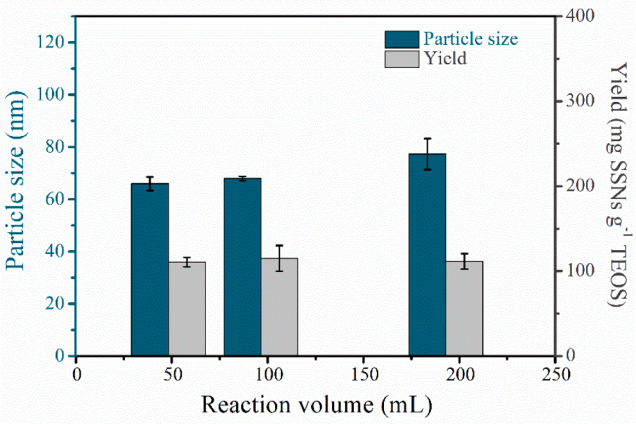

Fig. 4. Influence of reaction volume on SSN size (QELS) and yield. Conditions: various volumes of mixture (99.8 % ethanol/8.1 % NH_4OH/98.0 % TEOS/H_2O = 24.0:1.6:1.0:12.0 (volume)) were sonicated at 500 kHz, 207 W for 60 min at 20 °C in a 3 L water bath.

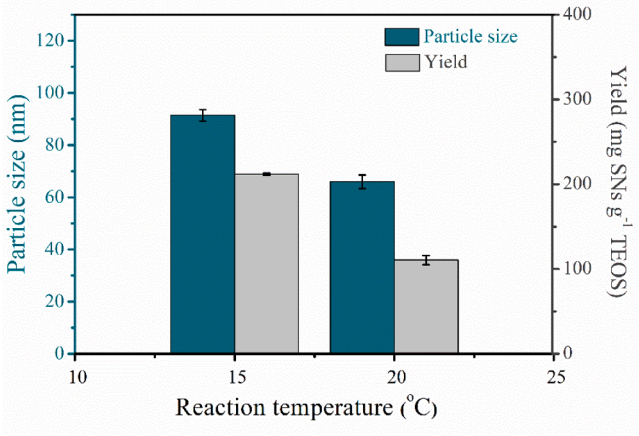

Fig. 5. Dependence of SSN size (QELS) and the yield on the reaction temperature. Conditions: ca. 50 mL of mixture (99.8 % ethanol: 30.00 mL; 8.1 % NH_4OH: 2.00 mL; 98.0 % TEOS: 1.25 mL; H_2O: 15.00 mL) was sonicated at 500 kHz, 207 W for 60 min in a 3 L water bath.

Generally, the number and size of cavitation bubbles increased with increasing bulk temperature [46,47]. Similarly to the effects of ultrasonic frequency and power, the increasing number of microbubbles generated at 20 °C resulted in smaller SSNs and lower yields. It is consistent with that the nucleation rate increased with increasing temperature [27,48]. The number of cavitation bubbles increased with increasing temperature, resulting in better dispersion of TEOS and ammonia and the decreasing concentration at nucleation sites, thereby dropping the yield of SSNs. Upon further increasing the temperature to 25 °C and 35 °C, the increasing number of bubbles decreased the concentration of TEOS and ammonia to a greater extent at nucleation sites, thereby limiting SSN formation with a lower initial ratio of NH_4OH/TEOS (0.84).

3.4. Influence of sonication time on SSN size and yield

Generally, the deposition thickness on the SSNs increases by unceasing hydrolysis and condensation with the sonication time [24]. As can be seen in Fig. 6, the SSN size increased, while the yields slightly fluctuated, with longer sonication at 500 kHz and 207 W at 20 °C.

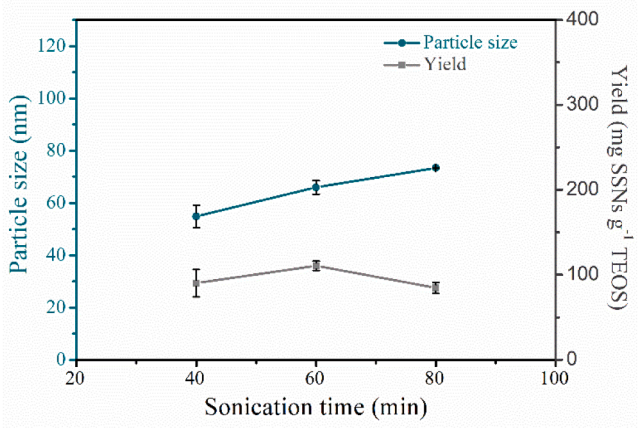

Fig. 6. Influence of sonication time on SSN size (QELS) and yield. Conditions: ca. 50 mL of mixture (99.8 % ethanol: 30.00 mL; 8.1 % NH_4OH: 2.00 mL; 98.0 % TEOS: 1.25 mL; H_2O: 15.00 mL) was sonicated at 500 kHz, 207 W at 20 °C in a 3 L water bath.

3.5. Further sonochemical mechanism dominating SSN size

To further probe the physicochemical effect of ammonia and ethanol on SSN formation, the amount of ammonia was reduced from 0.40 mL to 0.30 mL, and the amount of ethanol was decreased from 6.00 mL to 4.50 mL in the Stöber reaction system in separate experiments. Table 1 shows that no SSNs are obtained with the decreased levels of ammonia and ethanol in ca. 10 mL of the mixture under sonication at 500 kHz, 207 W for 20 min at 20 °C. This indicates that the proportions of both ammonia and ethanol are critical factors for SSN formation even under sonication, and that the active radicals generated during sonication may not be the driving factor for the process. To ascertain the role of these radicals, 10 μL of hydrophobic *n*-butanol was added into ca. 10 mL of the reaction mixture to scavenge the radicals generated in-situ during sonication at 500 kHz, 207 W for 20 min at 20 °C [49]. As shown in Table 1, the influence of *n*-butanol on SSN size (59 nm) and yield (172 mg SNs g^{-1} TEOS) was negligible.

The very high temperatures and pressures of collapsing gas bubbles lead to the thermal dissociation of water vapor into OH radicals and H atoms during the sonication. Both the formation of OH radicals and the role in the degradation of organics in aqueous solutions under sonication with various frequencies have been extensively demonstrated in previous works [30,44,50,51]. In 1996, Hoffmann *et al.* found that the degradation of TNT is more efficient at 500 kHz than at 20 kHz. The enhanced efficiency of irradiation at 500 kHz may be due to a higher rate of OH radicals production [51]. In 1997, Petrier and Francony reported the sonochemical degradation of phenol with different frequencies, 20, 200, 500, and 800 kHz. It was found that the reaction rates involving OH radicals (H_2O_2 formation and phenol degradation) have maximal values at 200 kHz, which was attributed to the better availability of OH radicals outside of the bubble of cavitation [44,52]. The electron paramagnetic resonance (EPR) is a highly sensitive method for measuring radicals and is a valuable tool for identifying the effect of OH radicals on the synthesis of SSNs. Fortunately, the dependence of OH radicals production detected by EPR on the sonication conditions, such as ultrasonic frequency and power, system temperature, dissolved gas, radical scavenger, as well as the configuration of ultrasonic reactors, has been very well known [53–57]. In 2001 and 2002, Topaz *et al.* reported the gradual increase of the DMPO-OH adduct signal with increasing sonication intensity with 20 kHz at 20 °C and at 40 kHz at 20 °C [55,56]. The similar results were also demonstrated by Režek Jambrak *et al.* recently [57]. Furthermore, Kubo *et al.* found that the concentration of DMPO-OH increases with the ultrasound power intensity (0.25–3 W cm^{-3}) at 50 kHz for 90 min at 20 °C, but it decreases with the reaction temperature (20–40 °C) with the ultrasonic power intensity of 1 W cm^{-3} at 50 kHz for 90 min [53]. In 2015, Zhang *et al.* comprehensively studied the effect of ultrasound frequency, power, temperature, etc., on the intensity of DMPO/1-hydroxylethyl free radical spin adducts in model wine. It demonstrated that the intensity of DMPO/1-hydroxylethyl free radical spin adducts increases with the increasing frequencies (45, 80, and 100 kHz) at 300 W and the increasing power (120, 180, 240, and 300 W) at 100 kHz for 5 min at 20 °C. Also, the intensity of free radical spin adducts in model wine increases with the increase of the system

Table 1
Effect of reducing ethanol and NH_4OH amount and adding *n*-butanol. Other conditions: ca. 10 mL of mixture, containing 3.00 mL of H_2O and 0.25 mL of TEOS, sonicated at 500 kHz and 207 W for 20 min at 20 °C in 3 L of water bath.

	Ethanol (mL)	8.1 % NH_4OH (mL)	*n*-butanol (μL)	Particle size (nm)	Yield (mg SSNs g^{-1} TEOS)
0	6.00	0.40	0	63 ± 3	155 ± 25
1	6.00	0.30	0	–	–
2	4.50	0.40	0	–	–
3	3.00	0.40	0	–	–
4	6.00	0.40	10	59 ± 2	172 ± 14

Note: The symbol "-" indicates that no SSNs formation was observed.

temperature from 20 to 50 °C at 100 kHz and 120 W for 5 min, then followed by a decrease at 60 °C [58]. Consequently, OH radicals can be formed in aqueous solution under the sonication, while more OH radicals yields with medium–high frequency sonication.

It can be speculated that rich OH radicals were produced at 500 kHz and 207 W at 20 °C in this study, however, the formed OH radicals should be immediately scavenged by ethanol in the reaction system. In 1983, Makino *et al.* found that alcohol, including methanol, ethanol, and butanol, in the aqueous solutions can effectively trap the radicals formed by the sonication (50 kHz and 60 mW cm^{-2}) by measuring the signal intensities of the spin adduct OH-DMPO [59]. It may be the reason that radicals do not play role in the sonochemical synthesis of SSNs with medium–high frequencies. On the other hand, it is known that *n*-butanol is an efficient OH radical scavenger in aqueous sonolysis, and adding *n*-butanol is able to confirm the OH radical-mediated reaction mechanism at the interface of the cavitation bubbles [60–62]. If the radicals play the role to a contain extent in the sonochemical synthesis of SSNs, the size and yield of SSNs should be strongly influenced in the presence of *n*-butanol due to the free radical scavenging effect. As listed in Table 1, the dominance of the radical mechanism was not observed in the

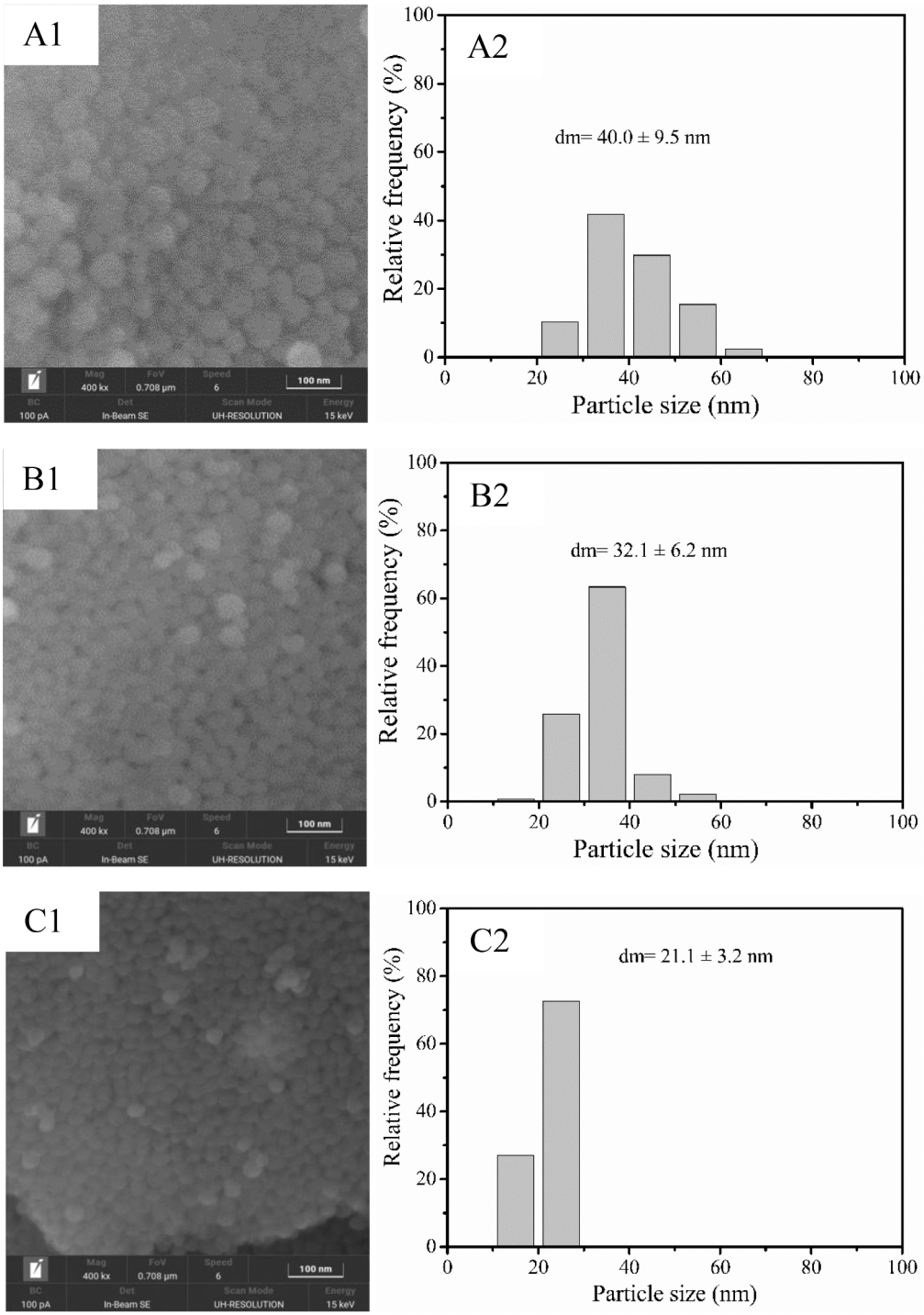

Fig. 7. FESEM images of the smallest SSNs obtained with sonication at (A1) 80 kHz, 63 W; (B1) 120 kHz, 78 W; and (C1) 500 kHz 207 W, and the particles size distribution of SSNs obtained with sonication at (A2) 80 kHz, 63 W; (B2) 120 kHz, 78 W; and (C2) 500 kHz, 207 W. Other conditions: ca. 10 mL of mixture (99.8 % ethanol: 6.00 mL, 8.1 % NH_4OH: 0.40 mL, 98.0 % TEOS: 0.25 mL, H_2O: 3.00 mL) was sonicated for 20 min at 20 °C in 3 L of water bath.

sonochemical synthesis of SSNs.

3.6. Characterization of SSNs

3.6.1. FESEM image and SSN size

Fig. 7 shows the FESEM images and size distributions of SSNs obtained under optimal sonication conditions with different ultrasonic frequencies.

As shown in Fig. 7, all the SSNs obtained under the medium–high frequency sonication exhibited spherical form and uniform distribution. The smallest average SSNs reached 40, 32, 21 nm under the optimal sonication conditions with 80, 120, and 500 kHz, respectively, and there the corresponding highest ultrasonic powers (63, 78, 207 W) were applied with various ultrasonic reactors.

It needs to note that the SSNs are directly dispersed in water after centrifugation without drying for the QELS analysis, whereas the SSNs are dried and dehydrated for the FESEM measurement. The rich Si–OH groups on the silica surface adsorb water molecules during the QELS measurement, leading to larger hydrodynamic diameter. In contrast, the SSN size decreases during the drying process. Therefore, the SSN size detected with FESEM is smaller than those detected with QELS.

3.6.2. FT-IR spectra of SSNs

FT-IR spectrum of the smallest SSNs obtained by sonication at 80 kHz, 120 kHz, and 500 kHz were shown in Fig. S2. The absorption band at 3371 cm^{-1} could be attributed to the stretching vibrations of the Si-OH groups in the SSNs structure [63]. The strong and broadband at 1067 cm^{-1} was assigned to Si-O-Si asymmetric stretching vibration and the absorption band at 798 cm^{-1} could be classified as Si-O-Si symmetric stretching vibration [63,64], therefore, the SSNs network structure was formed with condensation reaction. In addition, 946 cm^{-1} can be attributed to the silanol group [63,64]. The band position of the silica sample at 1634 cm^{-1} was attributed to the bending vibration of the H_2O 0.81 molecule in the Si-OH group [65]. The band position at 1067 cm^{-1} was slightly shifted to a lower wavenumber, due to the decreasing SSN size [66].

3.6.3. PXRD pattern of SSNs

To demonstrate the physical structure nature of SSNs, the sample synthesized by 500 kHz sonication was chosen for PXRD analysis. Fig. S3 shows the PXRD pattern of SSNs, which exhibits a broad and strong peak at $2\theta = 23.43^{\circ}$ without impurity peaks, indicating the amorphous nature of SSNs.

3.6.4. TGA of SSNs

Fig. S4 shows the TGA profiles of the smallest SSNs obtained by sonication at 80 kHz, 120 kHz, and 500 kHz. It can be seen that the weights of SSNs were lost by about 5.3 wt% (500 kHz), 6.1 wt% (120 kHz), and 5.2 wt% (80 kHz) at low temperatures (<120 °C) owing to the removal of absorbed water on SSNs surface. From 120 to 1000 °C, about 7.4 wt% (500 kHz), 6.1 wt% (120 kHz), and 4.6 wt% (80 kHz) weight loss of SSNs were attributed to Si–OH dehydration of SSNs. Furthermore, more weight of smaller SSNs was lost than that of larger SSNs due to the difference in silanols of SSNs.

4. Conclusions

In summary, the size of synthesized SSNs can be controlled by medium–high frequency sonication. Ultrasonic frequency, power and temperature significantly affect SSN size and yield. SSN size decreased with increasing ultrasonic power at various frequencies (80, 120, and 500 kHz). The hydrodynamic diameters of 63–117 nm of SSNs were obtained under sonication with 80, 120, and 500 kHz. Moreover, the SSNs obtained were smaller at 120 kHz than at 80 kHz in a multi-frequencies ultrasonic reactor, and the SSN size decreased with increasing ultrasonic power at 20 °C. With another 500 kHz ultrasonic bath, the optimal system temperature for producing smaller SSNs was proven to be 20 °C. Also, the SSN size decreased with increasing ultrasonic power. The smallest SSNs (63 nm, hydrodynamic diameter by QELS, or 21 nm by FESEM) were obtained by sonication at 207 W for 20 min at 20 °C.

The number of active sites or microbubbles increased with the increasing ultrasonic frequency and power, thus TEOS and ammonia were more evenly distributed around the active site, resulting in smaller SSNs. SSN-synthesis scale-up is feasible in the same ultrasonic reactor, while the synthesis efficiency slightly fluctuates over the 50–200 mL range. Similarly, the larger number of microbubbles were generated with increasing temperature from 15 to 20 °C resulted in smaller SSNs and lower yields. The particle size increased with the sonication time due to the increasing deposition thickness on the SSNs by unceasing hydrolysis and condensation with time. Moreover, the proportions of both ammonia and ethanol are critical factors for SSN formation even under sonication, and that the active radicals generated during sonication may not be involved in the process. Compared with the traditional Stöber or low-frequency-sonication methods, medium–high frequency sonication can significantly reduce reaction time and reagent amounts with a low molar ratio of NH_4OH/TEOS (0.84).

CRediT authorship contribution statement

Xiaolin Liu: Methodology, Writing – original draft. **Zhilin Wu:** Conceptualization, Data curation, Writing – original draft, Writing – review & editing, Supervision. **Maela Manzoli:** Methodology, Validation. **László Jicsinszky:** Methodology. **Roberta Cavalli:** Conceptualization, Data curation. **Luigi Battaglia:** Validation. **Giancarlo Cravotto:** Conceptualization, Writing – review & editing, Supervision.

Declaration of Competing Interest

The authors declare that they have no known competing financial interests or personal relationships that could have appeared to influence the work reported in this paper.

Data availability

No data was used for the research described in the article.

Acknowledgments

The China Scholarship Council and the University of Turin (Ricerca Locale 2021) are acknowledged for their financial support.

Appendix A. Supplementary data

Supplementary data to this article can be found online at https://doi.org/10.1016/j.ultsonch.2022.106181.

References

[1] F. Torney, B.G. Trewyn, V.-Y. Lin, K. Wang, Mesoporous silica nanoparticles deliver DNA and chemicals into plants, Nat. Nanotechnol. 2 (5) (2007) 295–300.
[2] S.E. Kim, L.i. Zhang, K. Ma, M. Riegman, F. Chen, I. Ingold, M. Conrad, M. Z. Turker, M. Gao, X. Jiang, S. Monette, M. Pauliah, M. Gonen, P. Zanzonico, T. Quinn, U. Wiesner, M.S. Bradbury, M. Overholtzer, others, Ultrasmall nanoparticles induce ferroptosis in nutrient-deprived cancer cells and suppress tumour growth, Nat. Nanotechnol. 11 (11) (2016) 977–985.
[3] M. Alqasaimeh, L.Y. Heng, M. Ahmad, A.S. Raj, T.L. Ling, A large response range reflectometric urea biosensor made from silica-gel nanoparticles, Sensors 14 (2014) 13186–13209.
[4] W. Stöber, A. Fink, E. Bohn, Controlled growth of monodisperse silica spheres in the micron size range, J. Colloid Interface Sci. 26 (1) (1968) 62–69.
[5] G.H. Bogush, M.A. Tracy, C.F. Zukoski, Preparation of monodisperse silica particles: control of size and mass fraction, J. Non-Cryst. Solids 104 (1) (1988) 95–106.
[6] I.A. Ibrahim, A. Zikry, M.A. Sharaf, Preparation of spherical silica nanoparticles: stober silica, J. Am. Sci. 6 (2010) 985–989.

[7] X.-D. Wang, Z.-X. Shen, T. Sang, X.-B. Cheng, M.-F. Li, L.-Y. Chen, Z.-S. Wang, Preparation of spherical silica particles by Stöber process with high concentration of tetra-ethyl-orthosilicate, J. Colloid Interface Sci. 341 (2010) 23–29.
[8] X. Liu, Z. Wu, R. Cavalli, G. Cravotto, Sonochemical preparation of inorganic nanoparticles and nanocomposites for drug release–A review, Ind. Eng. Chem. Res. 60 (28) (2021) 10011–10032.
[9] N.A. Dhas, K.S. Suslick, Sonochemical preparation of hollow nanospheres and hollow nanocrystals, J. Am. Chem. Soc. 127 (8) (2005) 2368–2369.
[10] A. Gedanken, Using sonochemistry for the fabrication of nanomaterials, Ultrason. Sonochem. 11 (2) (2004) 47–55.
[11] H. Xu, B.W. Zeiger, K.S. Suslick, Sonochemical synthesis of nanomaterials, Chem. Soc. Rev. 42 (7) (2013) 2555–2567.
[12] K.S. Suslick, Sonochemistry, Science 247 (4949) (1990) 1439–1445.
[13] K.S. Suslick, G.J. Price, Applications of ultrasound to materials chemistry, Annu. Rev. Mater. Sci. 29 (1) (1999) 295–326.
[14] S.L. Hem, The effect of ultrasonic vibrations on crystallization processes, Ultrasonics 5 (4) (1967) 202–207.
[15] C. Virone, H.J.M. Kramer, G.M. van Rosmalen, A.H. Stoop, T.W. Bakker, Primary nucleation induced by ultrasonic cavitation, J. Cryst. Growth 294 (1) (2006) 9–15.
[16] X. Zhang, T. Inada, A. Tezuka, Ultrasonic-induced nucleation of ice in water containing air bubbles, Ultrason. Sonochem. 10 (2) (2003) 71–76.
[17] P. Kanthale, M. Ashokkumar, F. Grieser, Sonoluminescence, sonochemistry (H_2O_2 yield) and bubble dynamics: frequency and power effects, Ultrason. Sonochem. 15 (2) (2008) 143–150.
[18] M. Ashokkumar, J. Lee, Y. Iida, K. Yasui, T. Kozuka, T. Tuziuti, A. Towata, Spatial distribution of acoustic cavitation bubbles at different ultrasound frequencies, ChemPhysChem 11 (8) (2010) 1680–1684.
[19] A. Brotchie, F. Grieser, M. Ashokkumar, Effect of power and frequency on bubble-size distributions in acoustic cavitation, Phys. Rev. Lett. 102 (2009), 084302.
[20] S. Merouani, O. Hamdaoui, Y. Rezgui, M. Guemini, Effects of ultrasound frequency and acoustic amplitude on the size of sonochemically active bubbles–theoretical study, Ultrason. Sonochem. 20 (3) (2013) 815–819.
[21] J. Lee, M. Ashokkumar, S. Kentish, F. Grieser, Determination of the size distribution of sonoluminescence bubbles in a pulsed acoustic field, J. Am. Chem. Soc. 127 (48) (2005) 16810–16811.
[22] A. Inui, A. Honda, S. Yamanaka, T. Ikeno, K. Yamamoto, Effect of ultrasonic frequency and surfactant addition on microcapsule destruction, Ultrason. Sonochem. 70 (2021), 105308.
[23] K. Yasui, Numerical simulations for sonochemistry, Ultrason. Sonochem. 78 (2021) 105728.
[24] N. Enomoto, T. Koyano, Z.-E. Nakagawa, Effect of ultrasound on synthesis of spherical silica, Ultrason. Sonochem. 3 (2) (1996) S105–S109.
[25] Z. Lin, Y. Wu, Y. Bi, Rapid synthesis of SiO_2 by ultrasonic-assisted Stober method as controlled and pH-sensitive drug delivery, J. Nanopart. Res. 20 (2018) 1–13.
[26] R. Kamila, Ridwan, M.P.M. Akhir, A. Patriati, A. Insani, Synthesis of silica particles through conventional sol-gel and sonochemistry methods and the effect of catalyst, water concentration and sample environment to the particle size, in, J. Phys. Conf. Series IOP Publish. 2193 (1) (2022) 012044.
[27] I. Rahman, P. Vejayakumaran, C. Sipaut, J. Ismail, M.A. Bakar, R. Adnan, C. Chee, An optimized sol-gel synthesis of stable primary equivalent silica particles, Colloids Surf. A 294 (2007) 102–110.
[28] H. Yao, J.-M. Hong, N. Li, S. Xu, J.-J. Zhu, Homogenous thionine-SiO_2 nanocomposite spheres: sonochemical preparation, characterization, and application in H_2O_2 biosensor, J. Nanosci. Nanotechnol. 9 (2009) 2421–2425.
[29] Q. Guo, D. Huang, X. Kou, W. Cao, L.u. Li, L. Ge, J. Li, Synthesis of disperse amorphous SiO_2 nanoparticles via sol–gel process, Ceram. Int. 43 (1) (2017) 192–196.
[30] Z.-L. Wu, J. Lifka, B. Ondruschka, Comparison of energy efficiency of various ultrasonic devices in aquasonochemical reactions, Chem. Eng. Technol. 29 (5) (2006) 610–615.
[31] R.F. Contamine, A.M. Wilhelm, J. Berlan, H. Delmas, Power measurement in sonochemistry, Ultrason. Sonochem. 2 (1) (1995) S43–S47.
[32] H. Tang, Y. Zhao, J.Z. Zhang, Y. Sha, L.G. Jin, Process research of amorphous SiO_2 for optical fiber preform by sol-gel, in, Adv. Mater. Res. Trans. Tech. Publ. (2011) 368–371.
[33] Z. Wu, B. Ondruschka, Roles of hydrophobicity and volatility of organic substrates on sonolytic kinetics in aqueous solutions, J. Phys. Chem. A 109 (29) (2005) 6521–6526.
[34] H.-M. Kim, C.-H. Lee, B. Kim, Sonochemical synthesis of silica particles and their size control, Appl. Surf. Sci. 380 (2016) 305–308.
[35] L. Cheng, J. Cai, Y. Ke, Ultrasonic-assisted sol–gel synthesis of core–shell silica particles for high-performance liquid chromatography, J. Inorg. Organomet. Polym. Mater. 30 (3) (2020) 859–868.
[36] S. Merouani, O. Hamdaoui, The size of active bubbles for the production of hydrogen in sonochemical reaction field, Ultrason. Sonochem. 32 (2016) 320–327.
[37] M. Gutierrez, A. Henglein, Chemical action of pulsed ultrasound: observation of an unprecedented intensity effect, J. Phys. Chem. 94 (1990) 3625–3628.
[38] K. Yasui, Influence of ultrasonic frequency on multibubble sonoluminescence, J. Acoust. Soc. Am. 112 (4) (2002) 1405–1413.
[39] F. Burdin, N.A. Tsochatzidis, P. Guiraud, A.M. Wilhelm, H. Delmas, Characterisation of the acoustic cavitation cloud by two laser techniques, Ultrason. Sonochem. 6 (1-2) (1999) 43–51.
[40] M. Ehsani, N. Zhu, H. Doan, A. Lohi, A. Abdelrasoul, In-situ synchrotron X-ray imaging of ultrasound (US)-generated bubbles: Influence of US frequency on microbubble cavitation for membrane fouling remediation, Ultrason. Sonochem. 77 (2021), 105697.
[41] R. Pflieger, A.A. Ndiaye, T. Chave, S.I. Nikitenko, Influence of ultrasonic frequency on Swan band sonoluminescence and sonochemical activity in aqueous tert-butyl alcohol solutions, J. Phys. Chem. B 119 (1) (2015) 284–290.
[42] S. Merouani, H. Ferkous, O. Hamdaoui, Y. Rezgui, M. Guemini, A method for predicting the number of active bubbles in sonochemical reactors, Ultrason. Sonochem. 22 (2015) 51–58.
[43] A. Dehane, S. Merouani, O. Hamdaoui, Effect of carbon tetrachloride (CCl_4) sonochemistry on the size of active bubbles for the production of reactive oxygen and chlorine species in acoustic cavitation field, Chem. Eng. J. 426 (2021), 130251.
[44] C. Pétrier, A. Francony, Ultrasonic waste-water treatment: incidence of ultrasonic frequency on the rate of phenol and carbon tetrachloride degradation, Ultrason. Sonochem. 4 (1997) 295–300.
[45] Y. Jiang, C. Petrier, T.D. Waite, Sonolysis of 4-chlorophenol in aqueous solution: effects of substrate concentration, aqueous temperature and ultrasonic frequency, Ultrason. Sonochem. 13 (2006) 415–422.
[46] S. Merouani, O. Hamdaoui, F. Saoudi, M. Chiha, Influence of experimental parameters on sonochemistry dosimetries: KI oxidation, Fricke reaction and H_2O_2 production, J. Hazard. Mater. 178 (2010) 1007–1014.
[47] H. Mulvana, E. Stride, J.V. Hajnal, R.J. Eckersley, Temperature dependent behavior of ultrasound contrast agents, Ultrasound Med. Biol. 36 (6) (2010) 925–934.
[48] S.K. Park, K. Do Kim, H.T. Kim, Preparation of silica nanoparticles: determination of the optimal synthesis conditions for small and uniform particles, Colloids Surf., A 197 (2002) 7–17.
[49] F. Grieser, R. Hobson, J. Sostaric, P. Mulvaney, Sonochemical reduction processes in aqueous colloidal systems, Ultrasonics 34 (2-5) (1996) 547–550.
[50] Z. Wu, G. Cravotto, M. Adrians, B. Ondruschka, W. Li, Critical factors in sonochemical degradation of fumaric acid, Ultrason. Sonochem. 27 (2015) 148–152.
[51] M.R. Hoffmann, I. Hua, R. Höchemer, Application of ultrasonic irradiation for the degradation of chemical contaminants in water, Ultrason. Sonochem. 3 (3) (1996) S163–S172.
[52] C. Petrier, A. Francony, Incidence of wave-frequency on the reaction rates during ultrasonic wastewater treatment, Water Sci. Technol. 35 (1997) 175–180.
[53] M. Kubo, K. Sekiguchi, N. Shibasaki-Kitakawa, T. Yonemoto, Kinetic model for formation of DMPO-OH in water under ultrasonic irradiation using EPR spin trapping method, Res. Chem. Intermed. 38 (9) (2012) 2191–2204.
[54] Z. Wei, F.A. Villamena, L.K. Weavers, Kinetics and mechanism of ultrasonic activation of persulfate: an in situ EPR spin trapping study, Environ. Sci. Technol. 51 (2017) 3410–3417.
[55] M. Topaz, M. Motiei, A. Gedanken, D. Meyerstein, N. Meyerstein, EPR analysis of radicals generated in ultrasound-assisted lipoplasty simulated environment, Ultrasound Med. Biol. 27 (6) (2001) 851–859.
[56] M. Topaz, M. Motiei, E. Assia, D. Meyerstein, N. Meyerstein, A. Gedanken, Acoustic cavitation in phacoemulsification: chemical effects, modes of action and cavitation index, Ultrasound Med. Biol. 28 (2002) 775–784.
[57] A. Režek Jambrak, S. Ojha, D. Šeremet, M. Nutrizio, N. Maltar-Strmecki, S. Vali, J. Gajdoš Kljusuri, B. Tiwari, Free radical detection in water after processing by means of high voltage electrical discharges and high power ultrasound, J. Food Process. Preserv. 45 (2021) e15176.
[58] Q.-A. Zhang, Y. Shen, X. Fan, J.F.G. Martin, X. Wang, Y. Song, Free radical generation induced by ultrasound in red wine and model wine: an EPR spin-trapping study, Ultrason. Sonochem. 27 (2015) 96–101.
[59] K. Makino, M.M. Mossoba, P. Riesz, Chemical effects of ultrasound on aqueous solutions. Formation of hydroxyl radicals and hydrogen atoms, J. Phys. Chem. 87 (8) (1983) 1369–1377.
[60] A.M. Lastre-Acosta, G. Cruz-González, L. Nuevas-Paz, U.J. Jáuregui-Haza, A.C.S. C. Teixeira, Ultrasonic degradation of sulfadiazine in aqueous solutions, Environ. Sci. Pollut. Res. 22 (2) (2015) 918–925.
[61] M.V. Bagal, P.R. Gogate, Sonochemical degradation of alachlor in the presence of process intensifying additives, Sep. Purif. Technol. 90 (2012) 92–100.
[62] N.B. Bokhale, S.D. Bomble, R.R. Dalbhanjan, D.D. Mahale, S.P. Hinge, B. S. Banerjee, A.V. Mohod, P.R. Gogate, Sonocatalytic and sonophotocatalytic degradation of rhodamine 6G containing wastewaters, Ultrason. Sonochem. 21 (5) (2014) 1797–1804.
[63] S. Musić, N. Filipović-Vinceković, L. Sekovanić, Precipitation of amorphous SiO_2 particles and their properties, Braz. J. Chem. Eng. 28 (1) (2011) 89–94.
[64] J.M. Kim, S.M. Chang, S.M. Kong, K.-S. Kim, J. Kim, W.-S. Kim, Control of hydroxyl group content in silica particle synthesized by the sol-precipitation process, Ceram. Int. 35 (3) (2009) 1015–1019.
[65] P.P. Nayak, A.K. Datta, Synthesis of SiO_2-nanoparticles from rice husk ash and its comparison with commercial amorphous silica through material characterization, Silicon 13 (4) (2021) 1209–1214.
[66] L. Singh, S. Agarwal, S. Bhattacharyya, U. Sharma, S. Ahalawat, Preparation of silica nanoparticles and its beneficial role in cementitious materials, Nanomater. Nanotechnol. 1 (2011) 9.